Journal of Biomolecular NMR (2005) 32: 101–111
DOI 10.1007/s10858-005-5094-5

Article

Can PISEMA experiments be used to extract structural parameters for mobile β-barrels?

Dustin W. Bleile, Walter R.P. Scott & Suzana K. Straus*
Department of Chemistry, University of British Columbia, 2036 Main Mall, Vancouver, B.C., V6T 1Z1, Canada.

Received 10 September 2004; Accepted 21 March 2005

Key words: mobility of membrane β-barrels, mosaic spread, PISEMA, time averaging

Abstract

The effect of mobility on ^{15}N chemical shift/^{15}N–^{1}H dipolar coupling (PISEMA) solid state NMR experiments applied to macroscopically oriented β-barrels is assessed using molecular dynamics simulation data of the NalP autotransporter domain embedded in a DMPC bilayer. In agreement with previous findings for α-helices, the fast librational motion of the peptide planes is found to have a considerable effect on the calculated PISEMA spectra. In addition, the dependence of the chemical shift anisotropy (CSA) and dipolar coupling parameters on the calculated spectra is evaluated specifically for the β-barrel case. It is found that the precise choice of the value of the CSA parameters σ_{11},σ_{22} and σ_{33} has only a minor effect, whereas the choice of the CSA parameter θ shifts the position of the peaks by up to 20 ppm and changes the overall shape of the spectrum significantly. As was found for α-helices, the choice of the NH bond distance has a large effect on the dipolar coupling constant used for the calculations. Overall, it is found that the alternating β-strands in the barrel occupy distinct regions of the PISEMA spectra, forming patterns which may prove useful in peak assignment.

Abbreviations: CS – chemical shift; CSA – chemical shift anisotropy; CS/D – ^{15}N chemical shift/^{15}N–^{1}H dipolar coupling; D – dipolar coupling; DMPC – dimyristoylphosphatidylcholine; MD – molecular dynamics; PISA – polarisation index of the slant angle; PISEMA – polarisation inversion spin exchange at the magic angle; r.m.s – root mean square.

Introduction

In the last decade, a number of solid state NMR techniques have been developed to obtain structural information on proteins which do not easily form crystals or are not amenable to the application of solution state NMR methods. Such systems include membrane proteins (Smith et al., 1996; Opella, 1997; Griffin, 1998; Davis and Auger, 1999; de Groot, 2000; Baldus, 2002) and other fibrous proteins, such as amyloids (Tycko, 2001), spider silk (van Beek et al., 2002), and cellulose (Maunu, 2002). For membrane proteins, in particular, a number of structures of integral α-helical membrane proteins (Opella et al., 1999; Song et al., 2000; Park et al., 2003; Gong et al., 2004) and bacteriophage particles (Zeri et al., 2003; Thiriot et al., 2004), which consist of repeating units of α-helices, have recently been elucidated using oriented solid state NMR. This methodology relies on the fact that the ^{15}N chemical shift and the ^{15}N–^{1}H dipolar splitting of the amide in the protein backbone are orientationally dependent in a macroscopically aligned sample. Both these parameters are extracted from a polarization

*To whom correspondence should be addressed. E-mail: sstraus@chem.ubc.ca

inversion spin exchange at the magic angle (PISEMA) spectrum (Ramamoorthy et al., 1999), which correlates the ^{15}N chemical shift and the ^{15}N–^{1}H dipolar splitting of all residues in a single experiment in a fully ^{15}N labelled protein. In an approach first proposed by Marassi and Opella (2000) and Wang et al. (2000), the assignment and determination of the orientation of each peptide plane in the protein is achieved by fitting the experimentally determined chemical shift/dipolar pair (CS/D) to calculated parameters (Marassi and Opella 2003). For α-helices, the calculated spectra are obtained using a static ideal α-helix ($\phi = -65°$, $\psi = -40°$) and consist of characteristic patterns, called PISA wheels, that mimic the helical wheel patterns first proposed by Schiffer and Edmundson (1967).

A number of α-helical membrane embedded proteins have been found to be dynamic in the pico- to micro-second timescales (Prosser and Davis, 1994; North and Cross, 1995; Huster et al., 2001) or to insert in the membrane with a large spatial orientational distribution or mosaic spread (Sizun and Bechinger, 2002; Kamihira et al., 2005). Consequently, we have recently investigated the effects of time and spatial averaging on PISEMA spectra (Straus et al., 2003), in order to determine whether the PISA wheel approach can easily be extended to more mobile/heterogeneous α-helical membrane proteins. We used molecular dynamics (MD) to simulate fast librational motion and uniform or Gaussian distributions to simulate rotational and tilt motion of the helix in order to assess the effect of mobility on the accuracy in determining configurational parameters, such as the helix tilt angle. The effect of dynamics, due to librational motion in particular, was found to be considerable on the position of calculated chemical shift/dipolar splitting pairs, as compared to those obtained using a static ideal helix. As a consequence, we proposed an alternate model to the static ideal helix model, which can be used to extract the helix tilt angle of a transmembrane helix for such systems.

In this contribution, we further investigate how the PISEMA experiment can be used to extract structural parameters of mobile β-barrels. For these systems, there is to date no experimentally determined structure based on PISEMA data. Theoretical spectra based on static structures of individual β-sheets (Marassi, 2001; Fares and Davis, 2003) and of complete β-barrels (Marassi, 2001; Vosegaard and Nielsen, 2002) have, however, been calculated. These studies have found characteristic patterns analogous to PISA wheels which could be used in assignment and structure determination. Since recent work has shown that β-barrels undergo motions in the nano- to microsecond regime and display a gradual increase in structural disorder from the center of the barrel to the loops (Fernandez et al., 2001; Fanucci et al., 2002; Hwang et al., 2002) we assess here the effects of librational motion using data obtained from a molecular dynamics simulation of the NalP autotransporter domain, whose structure was recently solved by X-ray crystallography to 2.6 Å resolution (Oomen et al., 2004), in an explicit DMPC bilayer. Unlike single transmembrane α-helices which can insert in a membrane bilayer at different angles, β-barrels are much larger and insert at angles only roughly parallel to the membrane normal. We therefore only consider the effects of small distributions in the tilt and rotation (in addition to librational motion) on the position of the chemical shift/dipolar pairs in the simulated PISEMA spectra.

Methods

The starting coordinates of the simulations were taken from an experimentally determined X-ray structure of the NalP autotransporter region (Oomen et al., 2004)(PDB entry 1UYN; resolution = 2.60 Å). The autotransporter section of the NalP protein consists of residues 777–1084, forming a 12 stranded, antiparallel transmembrane β-barrel with an α-helix running through the barrel centre (Figure 1). Missing atoms in residues 817, 919, 941, 946, 972, 999, 1055 and 1083 were modelled using Chimera (Pettersen et al., 2004). Three regions of the NalP autotransporter, residues 777–785, 943–945 and 1022–1038, were not observed in the crystal structure. Residues 777–785 were omitted from the simulation. The conformation of the missing residues 941–947 and 1020–1040 were generated using that of the residues 996–998 and 869–889, respectively, using Chimera (Pettersen et al., 2004).

The simulation was performed using the GROMOS96 (van Gunsteren et al., 1996; Scott et al., 1999) biomolecular program package using

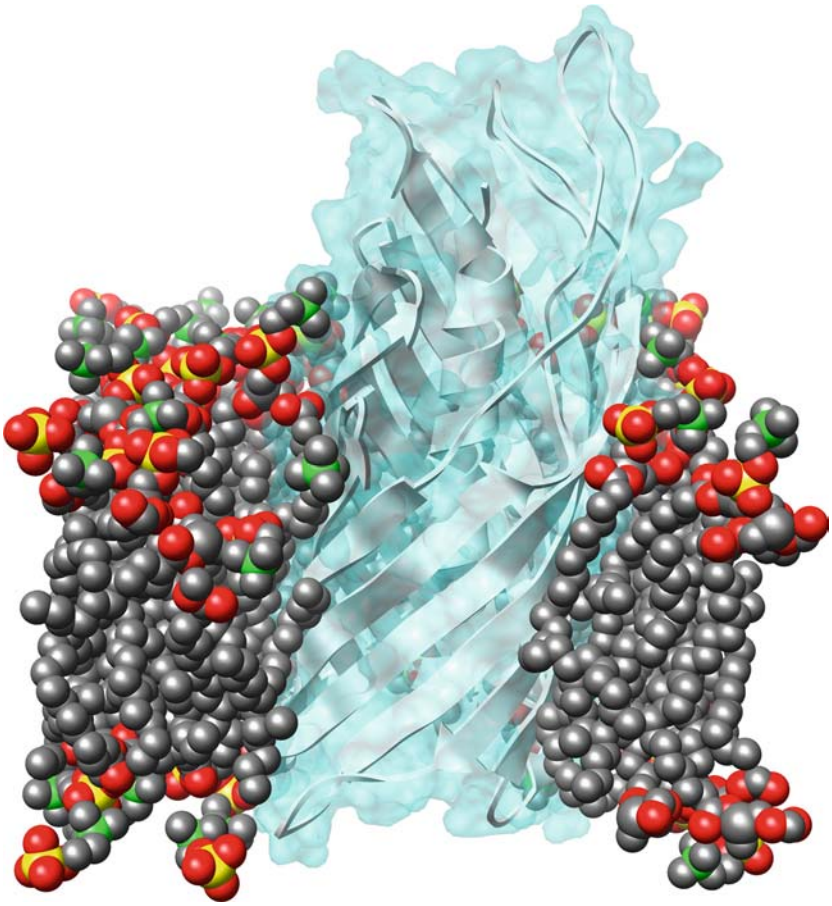

Figure 1. A view of the simulated NalP autotransporter domain in DMPC. Some of the lipids as well as the water have been omitted for clarity. This picture was generated using Chimera (Pettersen et al., 2004).

the 45A3 membrane force field (Chandrasekhar et al., 2003). The NalP β-barrel was placed in a previously equilibrated DMPC bilayer with SPC water (Berendsen et al., 1981). The positioning of the NalP protein within the bilayer was determined by inspection with the UCSF Chimera package (Pettersen et al., 2004) and adjusted to the expected depth (Oomen et al., 2004). Bilayer molecules containing atoms within 0.2 nm of the NalP protein were removed and additional water molecules added. This final system of 23,085 atoms then consists of a 299 residue protein in a bilayer of 79 DMPC and 5549 water molecules.

Simulations were performed in the NPT (300 K, 1 atm) ensemble with rectangular box periodic boundary conditions using the Berendsen coupling techniques (Berendsen et al., 1984). All covalent bonds were constrained with a relative geometric tolerance of 10^{-4} using the SHAKE method (Ryckaert et al., 1977). A reaction field long distance correction to the truncated Coulomb potential was applied (Tironi et al., 1995). After placement of the protein into the bilayer and solvation, the system was minimised with harmonic position restraints (force constant of 4000 kJ mol^{-1} nm^{-2}) on the C_α atoms. This final system was equilibrated for 5.5 ns with position restraints in place. Data collection simulations ensued from this equilibrated system without position restraints for 12 ns, from which 600 equidistant configurations were taken for data analysis. The r.m.s. deviations of the peptide plane angles in the β-sheet, α-helical and loop regions averaged 12°, 13° and 17°, respectively (data not shown). The r.m.s. deviation of the planes angles of the α-helix region is comparable

to those observed in a previous simulation (Straus et al., 2003). The positional r.m.s. deviation from the crystal structure was smaller than 1.6 Å, measured for the 189 β-sheet C_α atoms, throughout the simulation, which is comparable to similar simulations of β-barrels (Faraldo-Gomez et al., 2003).

In the PISEMA experiment, an instantaneous point $\nu_i(t) = ({}^{15}NCS_i(t), {}^{15}N - {}^{1}HD_i(t))$ is determined for each non-proline peptide plane i (Figure 2), for which the chemical shift (CS) and dipolar coupling (D) are determined from

$$\begin{aligned} {}^{15}NCS_i(t) =& \sigma_{11}\sin^2(\alpha_i(t) - \theta)\sin^2(\beta_i(t)) \\ &+ \sigma_{22}\cos^2(\beta_i(t)) \\ &+ \sigma_{33}\cos^2(\alpha_i(t) - \theta)\sin^2(\beta_i(t)) \quad (1) \end{aligned}$$

$${}^{15}N-{}^{1}HD_i(t) = \frac{b_{\mathrm{NH}}}{r_{\mathrm{NH}}^3}\left[3\cos^2(\alpha_i(t))\sin^2(\beta_i(t)) - 1\right]. \quad (2)$$

The angles α_i (t) and β_i (t) refer to the angle between the $N\vec{H}_i$ bond and the projection of the magnetic field vector $\vec{B}_0$ onto the peptide plane and the angle between $\vec{B}_0$ and the peptide plane normal $\vec{n}_i$, respectively. σ_{11}, σ_{22} and σ_{33} and the angle θ are experimentally determined CSA parameters. b_{NH} = 12171.5 Hz Å^3 is the NH dipolar coupling constant. r_{NH}^3 is the cube of the NH bond length. For this paper a value of r_{NH} = 1.066 Å averaged from experimental NMR data (Straus et al., 2003) was used.

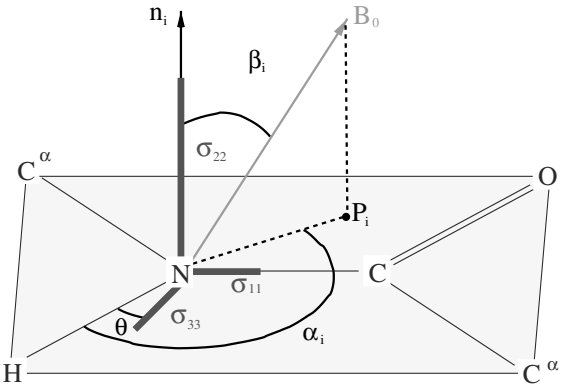

Figure 2. The definition of the plane variables used to calculate the chemical shift and dipolar splitting for a peptide plane.

In the calculations presented here, the following CSA parameters were used for non-glycine residues: σ_{11} = 61.6 ppm, σ_{22} = 83.0 ppm, σ_{33} = 223.6 ppm and θ = 16.7°. Since no θ values have been determined for non-glycine residues in a β-sheet conformation, the same value of θ as in (Straus et al., 2003) was used. For glycine residues, the corresponding parameters are: σ_{11} = 42.3 ppm, σ_{22} = 67.3 ppm, σ_{33} = 206.5 ppm and θ = 25°. These values were obtained from averaging literature values obtained for β-sheets only (see supplemental material). The CS/D points were calculated using the C program developed by Straus et al., (2003). The program was tested for correctness by comparing calculated spectra of porin (PDB 2POR) to literature values (data not shown).

For a β-barrel, an instantaneous ^{15}N chemical shift/^{15}N–^{1}H dipolar splitting pair (CS/D), $\nu_i(t) = (CS_i(t), D_i(t))$ is dependent on the following configurational variables:

- the angle ξ^{barrel} (t) between $\vec{B}_0$ and $\vec{n}^{\,\mathrm{barrel}}$, a vector parallel to the long barrel axis
- the angle of rotation $\omega^{\mathrm{barrel}(t)}$ about $\vec{n}^{\,\mathrm{barrel}}$ from a reference angle $\omega_0^{\mathrm{barrel}}$.
- the angle $\pi_i(t)$ between and the ith peptide plane and $\vec{n}^{\,\mathrm{barrel}}$.

Thus, now considering averaging effects, the observed NMR spectrum for peptide plane i will be determined by

$$\nu_i^{\mathrm{obs}} = \langle\{\nu_i(\xi^{\mathrm{barrel}}(t), \omega^{\mathrm{barrel}}(t), \pi_i(t))\}\rangle, \quad (3)$$

where ⟨⟩ and { } denote a time average and an average over all molecules, respectively.

The long axis $\vec{n}^{\,\mathrm{barrel}}$ was determined in the following way: under the assumption that the C_α positions in the β-barrel form a cylindrical shape, a circular pattern would be projected on to a plane whose normal was parallel to $\vec{n}^{\,\mathrm{barrel}}$. This plane was found by a random search, in which the deviation from the average projected C_α position distance to the in-plane C_α centre of mass was minimised. Only the C_α listed as belonging to SHEET in the 1UYN PDB entry were considered in this algorithm, using their positions from the minimised conformation. Subsequently, all trajec-

tory conformations were fitted to these same C_α carbons when calculating the ν_i^{obs}. The protein was not rotated about the barrel axis during this process, so ω_0^{barrel} was taken as the orientation found in the 1UYN PDB entry.

In order to calculate Equation 3 from computer simulation data, the correct distribution of the configurational parameters $\xi^{barrel}(t)$, $\omega^{barrel}(t)$, and $\pi_i(t)$ are needed. Given that β-barrels are large and have not been found to rearrange in the lipid bilayer rapidly (Fanucci et al., 2002), we assume that motions in ξ^{barrel} and ω^{barrel} are always slow on the NMR timescale. Thus we treat these two parameters as spatial distributions only. Since NalP consists of an α-helical segment as well as a β-barrel, we can use the librational motion of the peptide planes in the α-helix as a monitor of the librational amplitudes. Experimentally, these have been found to lie in the range of 5–16° (North and Cross, 1995; Huster et al., 2001). In the current simulations, the librational amplitudes for the α-helix are 10–12°, well within what is expected. Consequently, we consider the librational motion of the peptides planes observed in the simulation of the β-barrel, characterised by $\pi_i(t)$, to be fast on the NMR timescale and treat it as a time average, as in our previous work (Straus et al., 2003).

To verify that using a time-averaged $\pi_i(t)$ is a valid assumption, we also performed a 5 ns molecular dynamics simulation run (see supplemental material for computational details) of filamentous bacteriophage Pf1, calculated $\nu_i(\xi, \omega_0, <\pi_i(t)>)$ for each residue i, and compared to the assignments reported in the literature (Thiriot et al., 2004). The figure in the supplemental material shows that taking librational motion into account, by using MD simulation data, yields calculated $\nu_i(t) = (CS_i(t), D_i(t))$ which agree with experimental peak positions, within the error of the calculation (±5 ppm, ±200 Hz).

Finally, in order to determine the effect of each of the configurational parameters $\xi^{barrel}(t)$, $\omega^{barrel}(t)$ and $\pi_i(t)$, we therefore consider four combinations: (1) the static case; (2) librational motion alone, which is fast; (3) a combination of slow $\xi^{barrel}(t)$ motion with librational motion; and (4) a combination of slow $\omega^{barrel}(t)$ motion with librational motion (Table 1). As in previous work (Straus et al., 2003), equal intensities are assumed when spatial distributions are calculated and lines are drawn between data points to indicate allowed regions for the chosen distributions. In experimental spectra, the relative intensities of the points in the spatial distribution would correspond to the population density of molecules in the individual conformations.

Results

Case 1: Static β-barrel

The overall shape of the simulated PISEMA spectra for the static case ($\xi^{barrel} = \omega^{barrel} = 0°$) is oval, as emphasised by the solid demarcation line in Figure 3. Because of the different CSA parameter sets employed for non-glycine vs. glycine residues, two elliptical patterns are generated. On the left (greater CS) these two patterns overlap, while on the right the separation is clearly visible. When a single θ value is used for all amino acids, this shift disappears (not shown), and the spectra agree qualitatively with other calculated spectra in the literature (Marassi, 2001; Vosegaard and Nielsen, 2002). The PISEMA

Table S1. NMR averaging effects studied on the autotransporter region of NalP, where {} and < > denote averaging over slow and fast degree of freedom respectively

Case number	Variable parameters	Description
1	$\nu(\xi^{barrel} = 0°, \omega_0^{barrel}, \pi_{i_0})$	Static β-barrel
2	$\nu(\xi^{barrel} = 0°, \omega_0^{barrel}, <\pi_i(t)>)$	Fast planar motion only
3	$\nu(\{\xi^{barrel}(t)\}, \omega_0^{barrel}, <\pi_i(t)>)$	Slow ξ^{barrel} with fast planar motion
4	$\nu(\xi^{barrel} = 10°, \{\omega^{barrel}(t)\}, <\pi_i(t)>)$	Fixed ξ^{barrel} with slow ω^{barrel} and fast planar motion

$\xi^{barrel(t)}$ denotes the angle between the barrel axis and the membrane normal; $\omega^{barrel(t)}$ denotes a rotation around the barrel axis and $\pi_i(t)$ denotes the angle between peptide plane i and the barrel axis.

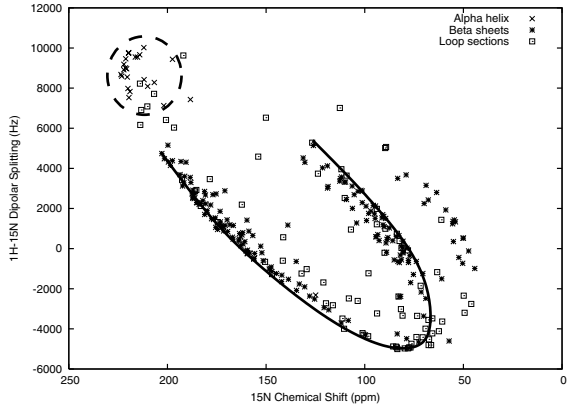

Figure 3. Calculated CS/D spectra of the autotransporter domain of NalP in the static case (case 1 in Table 1) for $\xi^{barrel} = \omega^{barrel} = 0°$. The protein consists of a transmembrane β-barrel (solid demarcation line) with a central α-helix (dashed circle region). The points to the right of the solid demarcation line are glycines (see text).

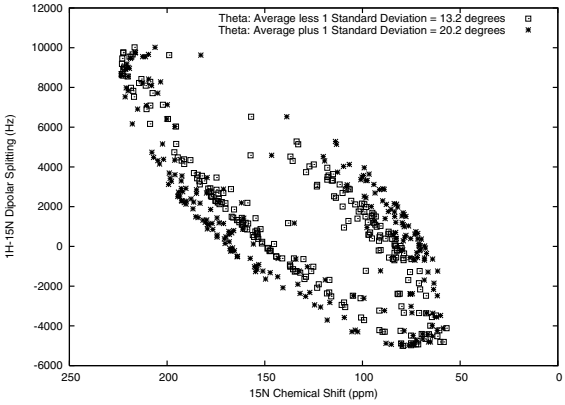

Figure 4. Effect of variation of θ on NalP PISEMA spectra (non-glycine residues only) in the static case and $\xi^{barrel} = \omega^{barrel} = 0°$. The two values for θ are 13.2° and 20.2°. The smaller θ value results in a noticeably more narrow oval shape.

points of the helix are clustered around the top left corner as expected (Straus et al., 2003) because the helix is oriented along the barrel axis. The PISEMA points of the β-barrel are mostly found on the edges of the ellipses, while the loop region points are scattered throughout the spectrum.

Variation of θ

As can be seen in Equation 1, θ influences the contributions of the σ_{11} and σ_{33} terms to the total CSA. As these two parameters typically differ by an order of magnitude, the choice of θ is critical. Unfortunately, θ is particularly badly defined due to lack of experimental data. The θ values are averaged from less than 10 sources for both the non-glycine and glycine residues and have a standard deviation of 3.5° from 16.7° average (non-glycines) and 2.7° from 21.6° (glycines) (Straus et al., 2003). Of all of these θ values, only a single glycine value was measured on a β-sheet.

In order to assess the sensitivity of the calculated CSA on variation of θ, we calculated the PISEMA spectra (static case) of the non-glycine residues for two values ($\theta_{big} = 16.7° + 3.5°$ and $\theta_{small} = 16.7° - 3.5°$) of θ (Figure 4). The smaller θ value noticeably reduces the spread of the points, resulting in a more narrow oval shape. The CS calculated with these separate θ values differ by up to 20 ppm.

Case 2: Librational motion only

The effects of fast librational motion on the simulated PISEMA spectra are shown in Figure 5, where the demarcations serve as a guide to compare to the static case (see caption). Here, the points have less range in both the CS and D directions. This averaging effect of librational motion is similar to what has been predicted and simulated in previous studies (Fares and Davis,

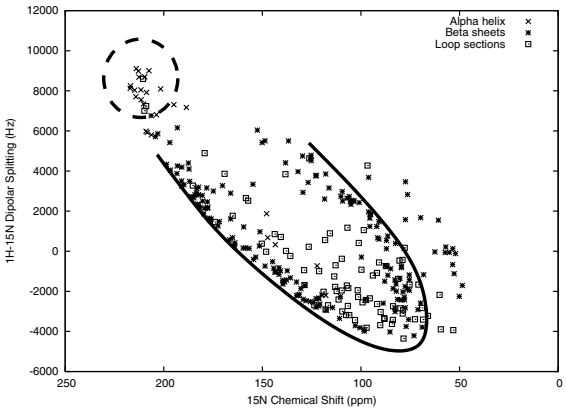

Figure 5. Simulated PISEMA for the autotransporter region of NalP with librational motion from a molecular dynamics simulation (case 2 in Table 1). The same region highlights as Figure 3 (dashed circle for α-helix, solid demarcation line for the β-barrel) are reproduced for comparison. Compared to the static case, the points have a smaller spread.

2003; Straus et al., 2003). The more mobile loop sections have the greatest differences between static and dynamic data. For the β-sheet sections, the average difference in CS from the static case is 14 ppm with a standard deviation of 13 ppm (data not shown). The D values of the β-sheet sections differ by an average of 1.6 kHz, with a standard deviation 1.1 kHz (data not shown). The librational influence on calculated CS and D values vary greatly with both the mobility and average orientation of the peptide planes.

Sequential spectral pattern

Knowing the approximate expected location of a peak can be useful in peak assignment. Typically, based on assumed regularity in structural motifs, it is possible to predict roughly where the peak of plane $n+1$ would lie given the location of the peak of plane n. For PISEMA spectra of helices, a circular pattern is assumed (Marassi, 2001), while for β-sheets more of a zig-zag pattern is predicted (Marassi, 2001; Fares and Davis, 2003), due to the alternating variation of peptide plane angles along the sheet.

Any such spectral pattern would be useful when faced with the daunting task of assigning the residues of a complete β-barrel. Here, we assess whether any general pattern can be discerned in the spectra, which might be useful in differentiating between individual sheets. Figure 6, in which the angles between the peptide planes and the barrel axis are plotted, shows that such a pattern indeed exists. The angles of the planes in adjacent β-strands are quite different from each other, forming an alternating pattern of positive and negative angles. In order to assess whether this is a general trait of β-barrels, a corresponding graph of porin (PDB entry 2POR) was calculated (see supplemental material). A similar pattern emerged.

Figure 7a and b (static, case 1 in Table 1) and 7c and d (librational motion only, case 2 in Table 1) shows a PISEMA spectra divided up according to even (starting on the extracellular side of the membrane) and odd (starting on the periplasmic side of the membrane) β-strands. Consecutive plane numbers are connected by lines. It can be seen that these lines run in opposing diagonal directions. When librational motion is considered, this pattern becomes clearer.

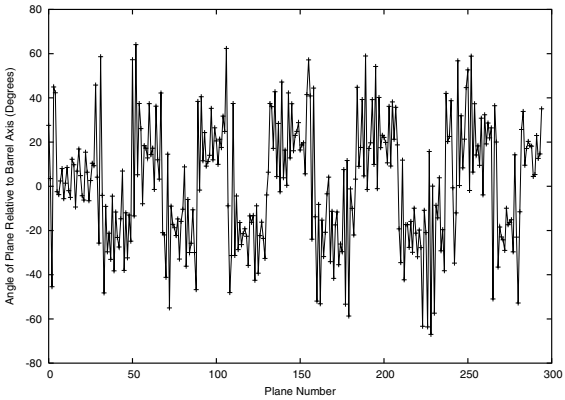

Figure 6. Average peptide plane angles relative to the barrel axis considering librational motion only (case 2 in Table 1). The plane numbering scheme starts at 0, corresponding to the peptide plane between residues 786 and 787 of NalP. The rest of the planes follow sequentially, except when proline residues (at positions 155, 207 and 250) are involved, in which case no plane angle is calculated. Plane numbers 0–25 are in the helix region. Plane numbers 236–252 are in the region of 1022–1038 in the sequence which was not present in the crystal structure. Overall, the alternating pattern of angles in the β-strands interspersed with the loop regions are easily discerned.

Case 3: Slow ξ^{barrel} motion with librational motion

Although transmembrane β-barrels are generally expected to be oriented with the barrel axis perpendicular to the bilayer, it is possible that small fluctuations in the axis tilt may occur. As we assume that the motions of such a large protein would be slow on an NMR timescale, an NMR experiment would detect the protein in a range of orientations. Figure 8 shows the PISEMA spectra for a single β-strand for ξ^{barrel} of 0°, 5° and 10°. The points of an individual plane are connected by lines to show their movements with the change in ξ^{barrel}. The effects are shown on a single β-strand for clarity. There is a very clear movement in most of the calculated PISEMA points.

Case 4: Fixed ξ^{barrel} with slow ω^{barrel} motion and librational motion

Rotation of the β-barrel about ω^{barrel} has no effect on $\pi_i(t)$ when $\xi^{\text{barrel}} = 0°$. However, for increasing values of ξ^{barrel}, the effect of ω^{barrel} becomes more pronounced on the calculated CS/D positions.

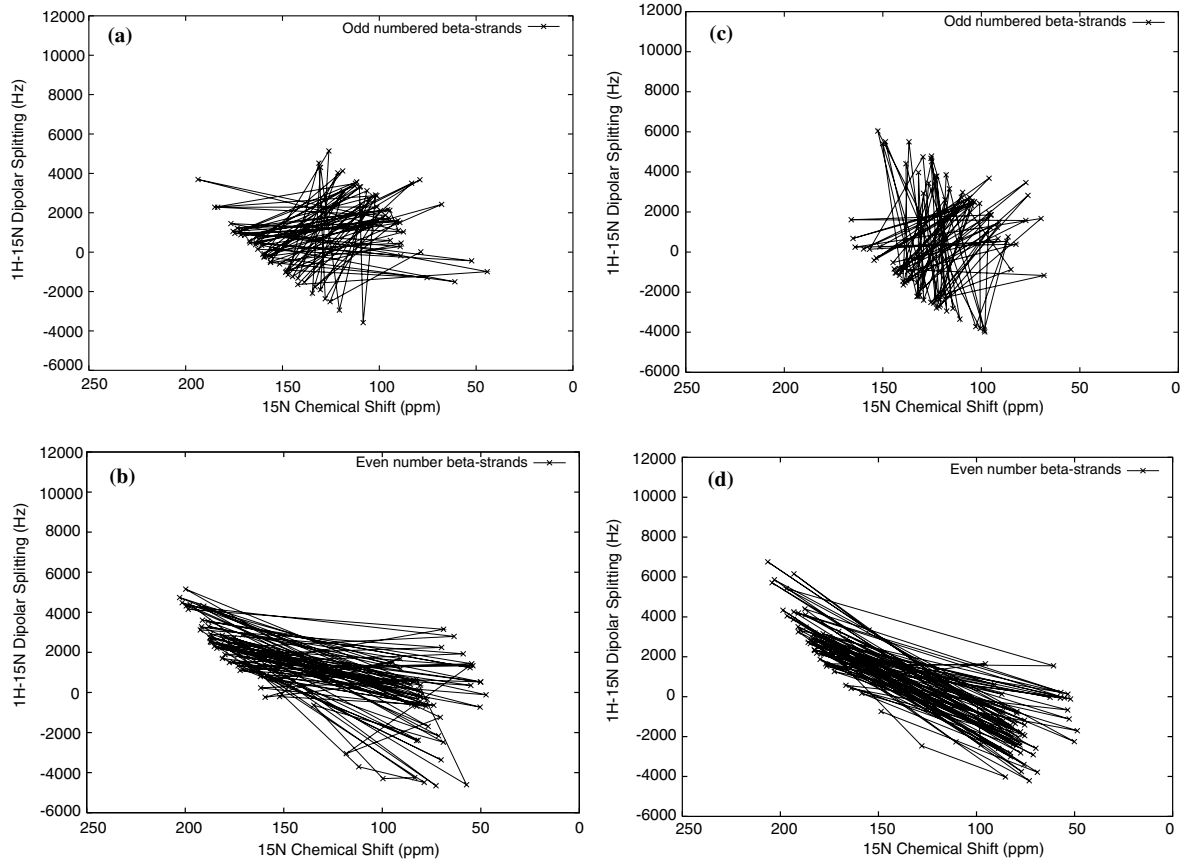

Figure 7. Simulated PISEMA of NalP (case 1 in Table 1 for a and b; case 2 in Table 1 for c and d). Sequentially ordered planes are connected by lines. The β-strands 1, 3, 5, 7, 9 and 11 starting on the periplasmic side of the membrane are plotted in a and c. The β-strands 2, 4, 6, 8, 10 and 12 starting on the extra-cellular side of the membrane are plotted in b and d. It can be seen that the even and odd numbered lines run in opposing diagonal directions. In case 2 compared to the static case, the pattern of opposing diagonal directions is more pronounced.

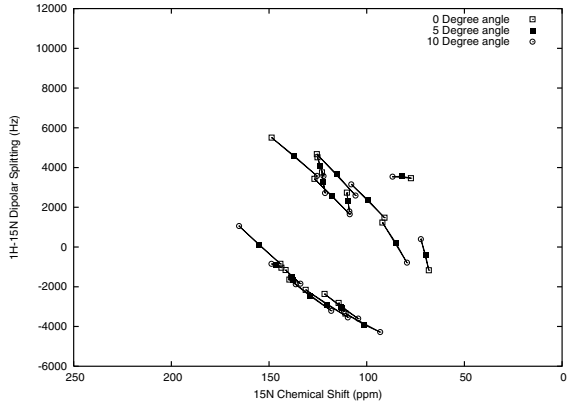

Figure 8. Simulated PISEMA spectra of a single β-strand (number 9) of NalP with $\xi^{barrel} = 0°$ (open squares), $\xi^{barrel} = 5°$ (filled squares) and $\xi^{barrel} = 10°$ (open circles) (case 3 in Table 1). There is a very clear movement in most of the calculated PISEMA points.

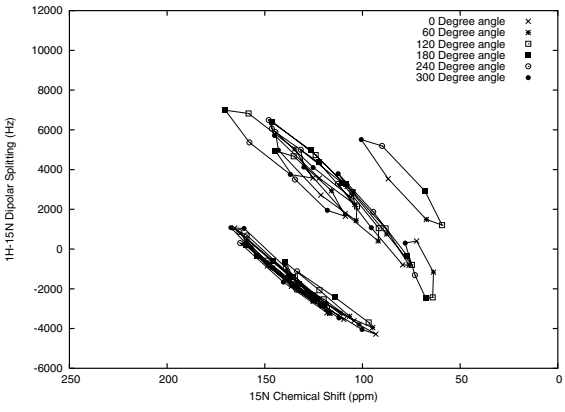

Figure 9. Simulated PISEMA spectra of a single β-strand (number 9) of NalP at $\xi^{barrel} = 10°$ and $\omega^{barrel} = n \times 60°$, where $n = 0$ (cross), $n = 1$ (star), $n = 2$ (open square), $n = 3$ (filled square), $n = 4$ (open circle) and $n = 5$ (filled circle) (case 4 in Table 1). At this value of ξ^{barrel}, the points are very sensitive to changes in ω^{barrel}.

In order to demonstrate this effect in what we consider an extreme case for transmembrane β-barrels, we set $\xi^{barrel} = 10°$ and plot an ω^{barrel} distribution of 0°, 60°, 120°, 180°, 240° and 300°. The resulting CS/D points, shown in Figure 9, are very sensitive to ω^{barrel}, tracing out elliptical or semi-elliptical patterns.

Discussion and conclusions

When calculating CS from Equation 1, σ_{11}, σ_{22} and σ_{33} and the angle θ are assumed to be constants, which is not strictly correct. In reality, these parameters are influenced by the electronic environment of the atoms in the residue. This in turn depends on the type and conformation of the residue in question and of those of neighbouring residues. Currently, only Ala, Val, Trp, Tyr and Gly have experimentally determined θ values (Straus et al., 2003). Another source of error is the use of an average, static N—H bond length when calculating D (Equation (2)). D has been shown to be very sensitive to the value of the N—H bond length (Straus et al., 2003). The use of a time-averaged bond length, instead of a time-dependent $r_{NH}(t)$ term, makes the incorrect assumption that $(\overline{r_{NH}})^3 = \overline{r_{NH}^3}$ for varying values of $r_{NH}(t)$. Since the motion of molecular bonds is poorly understood, the error introduced by this assumption is difficult to quantify. However, because bond stretching is very fast compared to other molecular motions, we suggest that this parameter can safely be assumed to be independent of the other variables and be modelled as a constant. In these simulations using bond constraints with SHAKE, this approximation is entirely appropriate, as the above assumption does hold for r_{NH} = constant.

When considering PISEMA spectra of transmembrane β-barrels compared to those of α-helices, a number of differences emerge. First, the overall motions, such as rotations or changes in tilt angle of the entire β-barrel, will be slower than single transmembrane helices in general because of the difference in size. This has an effect on the averaging properties of the spectra. Secondly, the range of tilt with respect to the membrane will likely be smaller for barrels. In general, membrane-bound barrels forming a channel are expected to have essentially $\xi^{barrel} = 0°$, at which a rotation around ω^{barrel} has no effect on the PISEMA spectra. This should facilitate the interpretation of spectra of β-barrels in practice. Thirdly, on the other hand, transmembrane β-barrels tend to be larger than single transmembrane α-helices, making the spectra more cluttered.

In general, the majority of the residues in the β-barrel fall on the 'twisted PISA wheel pattern' predicted for β-sheets tilted by 30–60° (Marassi, 2001) for $\xi^{barrel} = 0°$ and scatter throughout the allowed region when $\xi^{barrel} > 0$. The exceptions to this rule of thumb mostly involve residues in the highly mobile loop regions which are scattered throughout the allowed region for all ξ^{barrel} values. If the intensity of the observed CS/D for these regions is high, this would cloud the overall PISEMA pattern. We expect, however, that the mobile loop regions will not contribute significantly to the signal intensity, in which case they will not impede the observation of β-sheet regions.

Overall, the effects of librational motion on CS/D calculations are similar to those previously observed in α-helices (Straus et al., 2003). However, because the CS/D points for β-sheets generally lie in the 30–60° range, rather than at either close to 0° or 90° as in the case of α-helices, librational averaging effects can in contrast be seen to be beneficial in the β-barrel case. This is because averaging introduces only a small systematic error in the CS/D points in the 30–60° range.

Previously reported theoretical PISEMA patterns of antiparallel β-sheets had assumed that alternating β-strands lie in the same plane (Marassi, 2001; Fares and Davis, 2003). While this is likely appropriate for β-strands which do not form barrels, for the systems studied here (NalP and porin), we find that the average peptide plane angles of alternating β-strands are at an angle of approximately 40° to each other. Further investigation is required to determine whether this is a general feature of β-barrels. If confirmed, the resulting distinctive patterns in the PISEMA spectra would show some promise for structure determination.

In conclusion, the motional regimes investigated here are the most likely to have an effect on the position of chemical shift/dipolar splitting pairs in PISEMA spectra of mobile or heterogeneous macroscopically aligned β-barrel membrane

proteins, as seen from recent experimental data (Fernandez et al., 2001; Fanucci et al., 2002; Hwang et al., 2002). Of all types of motion studied here, fast librational motion of the peptide planes has a significant effect on the calculated PISEMA spectra and thus has to be taken into account when extracting structural parameters from such data. The observed difference in the angles of alternating β-strands may prove to be a useful tool in peak assignment in PISEMA spectra. Time will tell whether, once more experimental parameters appropriate for the β-sheet conformation are available, the PISEMA method is suitable for the study of membrane-bound β-barrels.

Acknowledgements

The provision of an equilibrated solvated bilayer of DMPC by I. Chandrasekhar (ETH Zürich) is gratefully acknowledged. We acknowledge Dr. D.A. Marvin (Cambridge) for an exciting and fruitful collaboration on Pf1. Useful discussions with James H. Davis (Guelph) are also gratefully acknowledged. WRPS acknowledges funding from the Canada Foundation for Innovation (CFI). SKS acknowledges funding from NSERC (University Faculty Award and Discovery Grant). The UCSF Chimera (Pettersen et al., 2004) package developed by the Computer Graphics Laboratory, University of California, San Francisco is supported by NIH P41 RR-01081.

Supporting information available

The following supporting information is available: a table of ^{15}N CSA parameters for β sheets for non-glycine residues, a table of ^{15}N CSA parameters for β sheets for glycine residues, a table of NH bond lengths, a plot of peptide plane angles relative to the *z*-axis for Porin (2POR.pdb), the initial configuration of Pf1 helices used for the molecular dynamics simulations, and finally a comparison of the simulated PISEMA spectrum of Pf1 from MD data with the assignment reported in (Thiriot et al., 2004). This material is available free of charge at http://dx.doi.org/10.1007/s10858-005-5094-5.

References

Baldus, M. (2002) *Prog. Nucl. Magn. Reson.*, **41**, 1–47.
Berendsen, H.J.C., Postma, J.P.M., van Gunsteren W.F., DiNola, A. and Haak, J.R., (1984) *J. Chem. Phys.*, **81**, 3684–3690.
Berendsen, H.J.C., Postma, J.P.M., van Gunsteren W.F. and Hermans, J. (1981) *Intermolecular Forces* Reidel, Dordrecht, pp. 331–342 Chapt. Interaction models for water in relation to protein hydration .
Chandrasekhar, I., Kastenholz, M., Lins, R.D., Oostenbrink, C., Schuler, L.D., Tieleman, D.P. and van Gunsteren W.F. (2003) *Eur. Biophys. J.*, **32**, 67–77.
Oomen, C.J., van, Ulsen P., van Gelder, P., Feijen, M., Tommassen, J. and Gros, P. (2004) *EMBO J.* **23**, 1257–1266.
Davis, J.H. and Auger, M. (1999) *Prog. Nucl. Magn. Reson.*, **35**, 1–84.
de Groot J.J.M. (2000) *Curr. Opin. Struct. Biol.*, **10**, 593–600.
Fanucci, G.E., Cadieux, N., Piedmont, C.A., Kadner, R.J. and Cafiso, D.S. (2002) *Biochemistry* **41**, 11543–11551.
Faraldo-Gomez, J.D., Smith, G.R. and Sansom, M.S.P. (2003) *Biophys. J.*, **85**, 1406–1420.
Fares, C. and Davis, J.H. (2003) *NMR of Ordered Liquids* Kluwer Academic, Amsterdam, pp. 191–213 Chapt. The search for high resolution NMR methods for membrane peptide structure.
Fernandez, C., Hilty, C., Bonjour, S., Adeishvili, K., Pervushin, K. and Wüthrich, K. (2001) *FEBS Lett.*, **504**, 173–178.
Gong, X.-M., Choi, J., Franzin, C.M., Zhai, D., Reed, J.C. and Marassi, F.M. (2004) *J. Biol. Chem.*, **279**, 28954–28960.
Griffin, R.G. (1998) *Nat. Struct. Biol.* **5**, 508–512.
Huster, D., Xiao, L. and Hong, M. (2001) *Biochemistry*, **40**, 7662–7674.
Hwang, P.M., Choy, W.Y., Lo, E.I., Chen, L., Forman-Kay, J.D., Raetz, C.R., Prive, G.G., Bishop, R.E. and Kay, L.E. (2002) *Proc. Natl. Acad. Sci. USA*, **99**, 13560–13565.
Kamihira, M., Voosegaard, T., Mason, A.J., Straus, S.K., Nielsen, N.C. and Watts, A. (2005) *J. Struct. Biol.*, **149**, 7–16.
Marassi, F. and Opella, S. (2003) *Protein Sci.*, **12,** 403–411.
Marassi, F.M. (2001) *Biophys. J.*, **80**, 994–1003.
Marassi, F.M. and Opella, S.J. (2000) *J. Magn. Reson.*, **144**, 150–155 .
Maunu, S.L. (2002) *Prog. Nucl. Magn. Reson.*, **40**, 151–174 .
North, C.L. and Cross, T.A. (1995) *Biochemistry*, **34**, 5883–5895.
Opella, S.J. (1997) *Nat. Struct. Biol.*, **4S**, 845–848.
Opella, S.J., Marassi, F.M., Gesell, J.J., Valente, A.P., Kim, Y., Oblatt-Montal, M. and Montal, M. (1999) *Nat. Struct. Biol.*, **6**, 374–379.
Park, S.H., Mrse, A.A., Nevzorov, A.A., Mesleh, M.F., Oblatt-Montal, M., Montal, M. and Opella, S.J., (2003) *J. Mol. Biol.*, **333**, 409–424.
Pettersen, E.F., Goddard, T.D., Huang, C.C., Couch, G.S., Greenblatt, D.M., Meng, E.C. and Ferrin, T.E. (2004) *J. Comput. Chem.*, **25**, 1605–1612.
Prosser, R.S. and Davis, J.H. (1994) *Biophys. J.*, **66**, 1429–1440.
Ramamoorthy, A., Wu, C.H. and Opella, S.J. (1999) *J. Magn. Reson.*, **140**, 131–140.
Ryckaert, J.-P., Ciccotti, G. and Berendsen, H.J.C. (1977) *J. Comput. Phys.*, **23**, 327–341.
Schiffer, M. and Edmundson, A.B. (1967) *Biophysical. J.*, **7**, 121–135.

Scott, W.R.P., Hünenberger, P.H., Tironi, I.G., Mark, A.E., Billeter, S.R., Fennen, J., Torda, A.E., Huber, T., Krüger, P. and van Gunsteren W.F. (1999) *J. Phys. Chem. A*, **103**, 3596–3607.

Sizun, C. and Bechinger, B. (2002) *J. Am. Chem. Soc.*, **124**, 1146–1147.

Smith, S.O., Aschheim, K.A. and Groesbeek, M. (1996) *Quart. Rev. Biophys.*, **29**, 395–449.

Song, Z.Y., Kovacs, F.A., Wang, J., Denny, J.K., Shekar, S.C., Quine, J.R. and Cross, T.A. (2000) *Biophys. J.*, **79**, 767–775.

Straus, S.K., Scott, W.R.P. and Watts, A. (2003) *J. Biomol. NMR*, **26**, 283–295.

Thiriot, D.S., Nevzerov, A.A., Zagyanskiy, L. Wu, C.H. and Opella, S.J. (2004) *J. Mol. Biol.*, **341**, 869–879.

Tironi, I.G., Sperb, R. Smith, P.E. and van Gunsteren W.F. (1995) *J. Chem. Phys.*, **102**, 5451–5459.

Tycko, R. (2001) *Ann. Rev. Phys. Chem.*, **52**, 575–606.

Beek, J.D. van Hess, S. Vollrath, F. and Meier, B.H. (2002) *Proc. Natl. Acad. Sci. USA*, **99**, 10266–10271.

van Gunsteren W.F., Billeter, S.R., Eising, A.A., Hünenberger, P.H., Krüger, P., Mark, A.E., Scott, W.R.P. and Tironi, I.G. (1996) *Biomolecular Simulation: The GROMOS96 Manual and User Guide* Zürich, GroningenVdF: Hochschulverlag AG an der ETH Zürich and BIOMOS b.v, ISBN 3 7281 2422 2.

Vosegaard, T. and Nielsen, N.C. (2002) *J. Biomol. NMR*, **22**, 225–247.

Wang, J., Denny, J., Tian, C., Kim, S., Mo, Y., Kovacs, F., Song, Z., Nishimura, K., Gan, Z., Fu, R., Quine, J.R. and Cross, T.A. (2000) *J. Magn. Reson.*, **144**, 162–167 .

Zeri, A.C., Mesleh, M.F., Nevzerov, A.A. and Opella, S.J. (2003) *Proc. Natl. Acad. Sci. USA*, **100**, 6458–6463.